

Quadrupole deformation of ^{16}C studied by proton and deuteron inelastic scattering

Y. Jiang,¹ J. L. Lou,^{1,*} Y. L. Ye,¹ Y. Liu,¹ Z. W. Tan,¹ W. Liu,¹ B. Yang,¹ L. C. Tao,¹ K. Ma,¹ Z. H. Li,¹ Q. T. Li,¹ X. F. Yang,¹ J. Y. Xu,¹ H. Z. Yu,¹ J. X. Han,¹ S. W. Bai,¹ S. W. Huang,¹ G. Li,¹ H. Y. Wu,¹ H. L. Zang,¹ J. Feng,¹ Z. Q. Chen,¹ Y. D. Chen,¹ Q. Yuan,¹ J. G. Li,¹ B. S. Hu,¹ F. R. Xu,¹ J. S. Wang,² Y. Y. Yang,² P. Ma,² Q. Hu,² Z. Bai,² Z. H. Gao,² F. F. Duan,² L. Y. Hu,³ J. H. Tan,³ S. Q. Sun,³ Y. S. Song,³ H. J. Ong,^{4,†} D. T. Tran,⁴ D. Y. Pang,⁵ and C. X. Yuan⁶

(RIBLL Collaboration)

¹*School of Physics and State Key Laboratory of Nuclear Physics and Technology, Peking University, Beijing 100871, China*

²*Institute of Modern Physics, China Academy of Science, Lanzhou 730000, China*

³*Fundamental Science on Nuclear Safety and Simulation Technology Laboratory, Harbin Engineering University, Harbin 150001, China*

⁴*Research Center for Nuclear Physics, Osaka University, Osaka 567-0047, Japan*

⁵*School of Physics, Beijing Key Laboratory of Advanced Nuclear Materials and Physics, Beihang University, Beijing 100191, China*

⁶*Sino-French Institute of Nuclear Engineering and Technology, Sun Yat-Sen University, Zhuhai 519082, China*



(Received 29 August 2019; accepted 23 January 2020; published 5 February 2020)

New measurements of proton/deuteron elastic and inelastic scattering to the 2_1^+ state of the neutron-rich nucleus ^{16}C have been performed at Radioactive Ion Beam Line in Lanzhou (RIBLL) in inverse kinematics. The angular distributions of elastic scattering were well reproduced by the systematic optical potential with normalization factors for the depths of real and imaginary parts. The neutron and proton deformation lengths of $\delta_n = 1.25 \pm 0.30$ fm and $\delta_p = 1.07 \pm 0.26$ fm were extracted from the inelastic scattering data. The ratio of neutron and proton matrix element $M_n/M_p = 1.95 \pm 0.47$ was determined from the two different probes. Within error bar, this result is in fair agreement with the previous measurements, demonstrating that the combination of proton and deuteron inelastic scattering offers a useful method to extract M_n/M_p for the even-even nuclei. Most of the theoretical predictions by the shell model using the MK, WBT, WBT*, and YSOX interactions in p - sd model space and by the *ab initio* in-medium similarity renormalization group are close to these experimental results.

DOI: [10.1103/PhysRevC.101.024601](https://doi.org/10.1103/PhysRevC.101.024601)

I. INTRODUCTION

Neutron-rich carbon isotopes have attracted a great deal of attention recently due to their abnormal shell structures [1–4] and exotic cluster structures [5–11]. For example, ^{15}C , ^{19}C , and the drip-line nucleus ^{22}C are proposed to be the neutron halo nuclei [1], while some high-lying unbound states in ^{14}C are suggested to have the linear-chain-configurations [8,9]. Deformation [12–14] plays an important role in the formation of these abnormal structures.

Quadrupole deformation in even-even nuclei, which represents the degree of nuclear collectivity, can be studied by observing the first 2^+ state. For the neutron-rich carbon isotopes, such as $^{16,18,20}\text{C}$, the 2_1^+ states have been widely studied by various experiments [15–24]. The relative neutron and proton contributions to the excitation of the 2_1^+ state can be described by the ratio of neutron and proton matrix elements $M_n/M_p = N\delta_n/(Z\delta_p)$, where δ_n and δ_p are the neutron and proton deformation lengths, respectively [25]. This ratio is usually equal to N/Z for most stable nuclei, but often larger or smaller than N/Z for neutron- or proton-rich nuclei, such as ^{20}O [26,27], ^{20}Mg [28,29], ^{32}Mg [30], ^{38}S [31],

and ^{74}Zn [32]. In principle, two experimental probes with different sensitivities to proton and neutron contributions are required to determine M_n/M_p . From experimental observables of electromagnetic transition, such as the reduced electric quadrupole transition probability, $B(E2)$, one can directly determine the M_p value with the following function [25]:

$$B(E2, J_i^+ \rightarrow 0^+) = e^2 \frac{M_p^2}{2J_i + 1}. \quad (1)$$

The proton deformation length δ_p is related to M_p as

$$\delta_p = \frac{4\pi}{3ZR^2} M_p = \frac{4\pi}{3ZR^2} \left[\frac{B(E2; 2_1^+ \rightarrow 0_{\text{g.s.}}^+)/e^2}{5} \right]^{1/2}. \quad (2)$$

The $B(E2)$ of an even-even unstable nucleus is often determined from the lifetime measurement of the 2_1^+ state using different experimental techniques, such as delayed coincidence, Doppler shift, pulsed beam, as well as recoil distance [33]. Inelastic scattering of nucleons or heavy ions, such as proton, neutron, deuteron, ^{12}C , and lead (Pb), also provide useful probes for determining M_n/M_p . The matter deformation length, δ_m^F , is usually extracted from normalizing the theoretical calculations to the inelastic scattering differential cross sections (DCSSs) for a probe F . δ_m^F is associated with M_n/M_p and the interaction strength between the probe and

*jllou@pku.edu.cn

[†]Present address: Institute of Modern Physics, Chinese Academy of Sciences, Lanzhou 730000, China.

TABLE I. For the 2_1^+ state in ^{16}C , a summary table of the experimental methods, results, and the corresponding M_n/M_p .

Measurement methods	Deformation length δ_n (fm)	Deformation length δ_p (fm)	M_n/M_p ^a
Inelastic scattering: Pb	1.9 ± 0.2	0.42 ± 0.05	7.6 ± 1.7 [16]
Inelastic scattering: Pb (AMD model) ^b	1.74	0.69	4.19 [34]
Inelastic scattering: proton	$\delta_m^p = 1.44 \pm 0.17$		6.7 ± 1.3 ^c [17]
Inelastic scattering: proton+Pb	1.37 ± 0.12	0.90 ± 0.13	2.54 ± 0.37 [20]
Present: proton+deuteron	1.25 ± 0.30	1.07 ± 0.26	1.95 ± 0.47
Measurement methods	$B(E2; 2_1^+ \rightarrow 0_{\text{g.s.}}) (e^2 \text{ fm}^4)$	δ_p (fm) ^d	M_n/M_p ^e
Lifetime: recoil shadow	0.63 ± 0.12	0.41 ± 0.06	6.7 ± 1.3 [15,17]
Lifetime: upgraded recoil shadow	$2.6 \pm 0.2 \pm 0.7^f$	0.83 ± 0.3	3.31 ± 0.75 [17,18]
Lifetime: recoil distance	4.15 ± 0.73	1.05 ± 0.18	2.40 ± 0.41 [17,19]
Lifetime: recoil distance	$4.21^{+0.34}_{-0.26}(\text{stat})^{+0.28}_{-0.24}(\text{syst}_{B\rho})$	1.06 ± 0.12	2.40 ± 0.28 [17,21]
Present: proton+deuteron	$4.34^{+2.27}_{-1.85}$	$\delta_p = 1.07 \pm 0.26$	1.95 ± 0.47

^aDetermined using the equation of $M_n/M_p = (N\delta_n/Z\delta_p)$.

^b δ_p is calculated from the $B(E2; 2_1^+ \rightarrow 0_{\text{g.s.}}^+) = 1.90 e^2 \text{ fm}^4$ with Eq. (2). M_n/M_p is deduced using $M_n = 13.0 \text{ fm}$ and $M_p = 3.1 \text{ fm}$.

^cCalculated from $\delta_m^p = 1.44 \pm 0.17 \text{ fm}$ [17] and $\delta_p = 0.41 \pm 0.06 \text{ fm}$ [15] using Eq. (3).

^dDeduced from the $B(E2; 2_1^+ \rightarrow 0_{\text{g.s.}}^+)$ values with Eq. (2).

^eThe $\delta_m^p = 1.44 \pm 0.17 \text{ fm}$ [17] and δ_p calculated from different $B(E2; 2_1^+ \rightarrow 0_{\text{g.s.}}^+)$ values were applied.

^fThe mean value from three different lifetime measurements, including the inelastic scattering of ^{16}C on ^9Be at 72 MeV/nucleon, the breakup of ^{18}C at 79 MeV/nucleon, and the angular distributions of the γ rays emitted from the 2_1^+ state in ^{16}C inelastically scattered on ^9Be at 40 MeV/nucleon [18].

neutrons (protons), b_n^F (b_p^F) [25],

$$\frac{\delta_m^F}{\delta_p} = \frac{1 + (b_n^F/b_p^F)(M_n/M_p)}{1 + (b_n^F/b_p^F)(N/Z)}. \quad (3)$$

For ^{16}C , several experiments have been carried out to disentangle the proton and neutron contributions to the 2_1^+ state. The different experimental methods and results are summarized in Table I. A very small $B(E2; 2_1^+ \rightarrow 0_{\text{g.s.}}^+)$ value of $0.63 \pm 0.12 e^2 \text{ fm}^4$ was first determined from the recoil shadow method with a theoretically calculated angular distributions of the 1766-keV γ rays emitted from the 2_1^+ state [15]. Later, this value was revised to be $2.6 \pm 0.2 \pm 0.7 e^2 \text{ fm}^4$ in a series of measurements where the 1766-keV γ -rays angular distributions were also measured [18]. Recently, from two different half-time measurements with the recoil distant method, $B(E2; 2_1^+ \rightarrow 0_{\text{g.s.}}^+)$ were determined to be $4.15 \pm 0.73 e^2 \text{ fm}^4$ [19] and $4.21^{+0.34}_{-0.26}(\text{stat})^{+0.28}_{-0.24}(\text{syst}_{B\rho}) e^2 \text{ fm}^4$ [21], which are consistent with the revised value of $2.6 \pm 0.2 \pm 0.7 e^2 \text{ fm}^4$. Until now, for the 2_1^+ state, the proton contributions, namely, M_p and δ_p were obtained.

However, comparing to M_p and δ_p , the experimental results on direct determination of M_n and δ_n were scarce. The matter deformation-length parameter $\delta_m^p = 1.44 \pm 0.17 \text{ fm}$ was obtained from the inelastic proton scattering of ^{16}C [17]. Together with $\delta_p = 1.05 \pm 0.18 \text{ fm}$ [19], M_n/M_p was deduced to be about $2.4 \approx 1.44 N/Z$, which is close to that of the neighboring nucleus ^{18}O , and is consistent with the global systematics for even-even nuclei [19]. From the inelastic scattering of ^{16}C from the Pb target, the anomalously large ratio of $M_n/M_p = 7.6 \pm 1.7 = 4.56 N/Z$ was deduced [16], which suggests that this 2_1^+ state is nearly a pure valence neutron excitation, and supports an interpretation of ‘‘decoupled’’ valence neutron in ^{16}C . However, the M_n/M_p value obtained

from the Pb target is sensitive to the choice of optical potential parameters and theoretical models. A subsequent analysis using the microscopic antisymmetrized molecular dynamics (AMD) model reported a relatively small value of $M_n/M_p = 4.15$ [34]. In addition, a simultaneous reanalysis for the previously determined integrated, total reaction cross sections (TRCSs) from proton [17] and Pb [16] inelastic scattering data gave a much smaller value of $M_n/M_p = 2.54 \pm 0.37$ [20]. To sum up, from the inelastic scattering of ^{16}C on proton and Pb, the deduced ratio of M_n/M_p changes nearly three times, from 2.4 to 7.6 using different analyzing methods. Therefore, more inelastic scattering data of ^{16}C on different targets (probes) are required to examine and determine M_n/M_p , especially M_n and δ_n .

In this paper, we report on a new proton/deuteron elastic and inelastic scattering experiment performed in inverse kinematics using a radioactive beam ^{16}C at about 24 MeV/nucleon. The elastic and inelastic scattering channels were successfully separated from the Q -value spectra obtained from the energies and angles of the recoil protons/deuterons in coincidence with ^{16}C . The elastic scattering data were used to extract the appropriate optical potential parameters, and to re-examine the large diffuseness parameters of imaginary part, which were obtained from the elastic scattering angular distributions of $^{16}\text{C} + p$ and $^{16}\text{C} + d$ at 50 MeV/nucleon [35]. The deformation parameters of neutron and proton were determined from the inelastic scattering data. Simultaneous use of the two different probes, proton and deuteron, allows us to extract the ratio of the neutron to proton matrix element M_n/M_p independent of any other experimental results. The M_n/M_p value was compared with shell model calculations using different interactions, and also with the *ab initio* calculations using in-medium similarity renormalization group (IM-SRG).

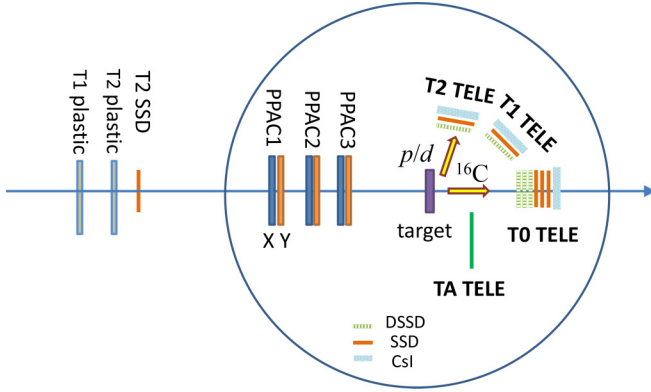


FIG. 1. The schematic view of experimental setup.

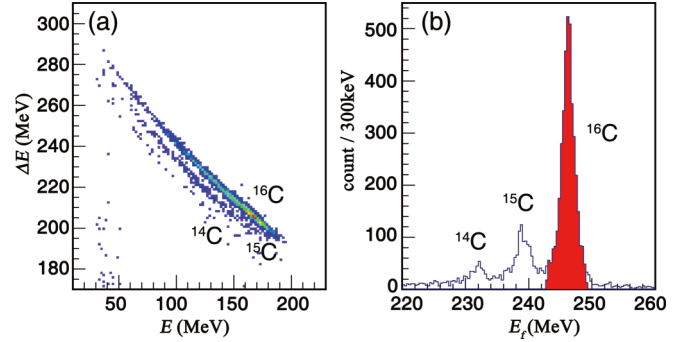
II. EXPERIMENT

A. Experimental setup

The experiment was performed at Radioactive Ion Beam Line in Lanzhou (RIBLL), Institute of Modern Physics (IMP), China. A ^{16}C secondary beam at about 24.0 MeV/nucleon was produced from a ^{18}O primary beam at 59.6 MeV/nucleon impinging on a ^9Be target with a thickness of 4.5 mm. The secondary beam was purified by a uniform 650- μm aluminum degrader, and was identified by the time-of-flight (TOF) provided by two plastic scintillator detectors and energy losses (ΔE) in a large-surface silicon detector (SSD). The average beam intensity and the purity of ^{16}C were up to 10^4 particles per second (pps) and 90%, respectively.

The experimental setup is schematically shown in Fig. 1. Three parallel plate avalanche counters (PPACs) were installed upstream of targets to provide beam tracking information, with a resolution of the hit position on the target less than 1.0 mm. A $4.37 \pm 0.05 \text{ mg/cm}^2$ $(\text{CH}_2)_n$ target and a $9.53 \pm 0.12 \text{ mg/cm}^2$ $(\text{CD}_2)_n$ target (where ‘D’ denotes ^2H) were used to measure the protons and deuterons scattering data, respectively. The $(\text{CH}_2)_n$ target was rotated 20° with respect to the beam direction in order to reduce the energy losses of the recoil protons in the target, while the $(\text{CD}_2)_n$ target was perpendicular to the beam direction due to requirements of other reaction channels. A $13.73 \pm 0.13 \text{ mg/cm}^2$ carbon target was employed to subtract the background coming from carbon atoms in the $(\text{CH}_2)_n$ and $(\text{CD}_2)_n$ targets. Data were also collected in an empty target run to measure random or accidental coincidence events.

A set of double-sided annular silicon strip detector TA, as well as five telescopes named T0, T1UP, T1DOWN, T2UP, and T2DOWN, were used in this experiment to detect and identify the charged particles with standard ΔE - E methods. In this paper, for the elastic and inelastic scattering channels, we only focused on the T0 and T2 (including T2UP and T2DOWN), which were placed 156 and 157 mm from the target to distinguish carbon isotopes around 0° and the scattered protons/deuterons, respectively. The telescope T0 consists of three 1000- μm -thick double-sided silicon strip detectors (DSSDs), three 1500- μm -thick SSDs, and a layer of 4-cm-thick CsI(Tl) crystals read out by photodiodes. The complicated T0 was specially designed for the measurement


 FIG. 2. With coincidence of the light-charged particles detected by the telescope T2, particle identification (PID) spectrum (a) and its linearization and projection spectrum (b) measured by the telescope T0. The data were taken from the $(\text{CD}_2)_n$ target.

of two-body fragments breakup from the high-lying cluster states in ^{16}C , and the experimental results will be published in other papers. The telescope T2, which was composed of a 300- μm -thick DSSD, a 1500- μm -thick SSD, and a layer of CsI(Tl) crystals, was placed at around 69° with respect to the beam direction. Each DSSD is divided into 32 strips on both sides and has an active area of $63.96 \times 63.96 \text{ mm}^2$. The telescope T0 and T2 cover scattering angles of $\theta_{\text{lab}}^{T0} = 0$ – 12° and $\theta_{\text{lab}}^{T2} = 57$ – 82° , respectively. Taking into account the position resolution resulting from PPACs ($\sim 1 \text{ mm}$) and DSSDs ($\sim 2 \text{ mm}$), the overall angular resolution of the telescope T2 was approximately 0.92° (FWHM). Except for the T0 and T2, other telescopes were employed to detect transfer reaction channels, such as $^{16}\text{C}(d, ^3\text{He})$ and $^{16}\text{C}(d, ^4\text{He})$, thus their details are not described in this paper.

B. Kinematics

The present experiment was performed in inverse kinematics, in which discrimination of various reaction channels (or of each populated state in the same channel) was achieved, using a same approach described in Refs. [36–39], by a coincidence measurement between the target-like particles (protons or deuterons) and the projectile-like fragments (carbon isotopes).

The particle identification (PID) spectra, which were obtained from the telescope T0 in coincidence with the recoil light-charged particles detected by the telescope T2, are shown in Fig. 2. Figure 2(a) shows the ΔE - E spectrum taken from the energy losses in the first two layer DSSDs of the T0. The carbon isotopes ^{16}C , ^{15}C , and ^{14}C can be discriminated clearly. ^{16}C ions are mainly from the elastic or inelastic scattering to the bound states at $E_x = 1.766 \text{ MeV}$ (2_1^+), $E_x = 3.986, 4.088, 4.142 \text{ MeV}$ in ^{16}C , while ^{15}C and ^{14}C particles come from inelastic scattering to the unbound states with excitation energies above $1n$ ($S_n = 4.25 \text{ MeV}$) and $2n$ separation threshold ($S_{2n} = 5.468 \text{ MeV}$), respectively. It should be noted that the second 0^+ state at around $E_x = 3.027 \text{ MeV}$ was hardly populated by the inelastic scattering [18]. In order to exactly choose carbon isotopes (^{16}C , ^{15}C , or ^{14}C) to discriminate different reaction channels, a standard linearization and projection procedure was applied to the ΔE - E spectrum using the method described in Ref. [40], and the result is

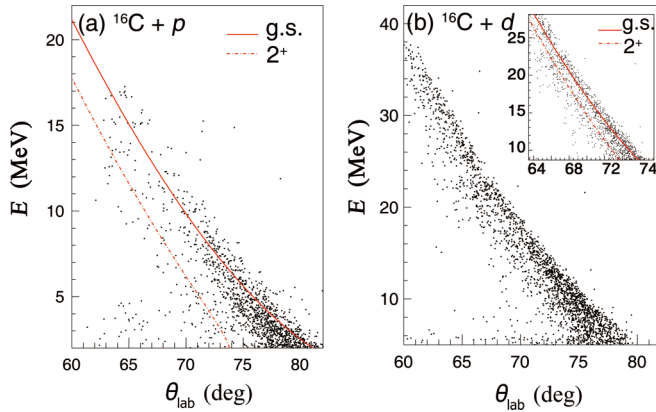


FIG. 3. Kinematics for the recoil protons (a) and deuterons (b) from the $(\text{CH}_2)_n$ and $(\text{CD}_2)_n$ targets, respectively. The solid and dot-dashed lines are the calculated kinematical curves for the elastic scattering and inelastic scattering to the 2_1^+ state at $E_x = 1.766$ MeV in the neutron-rich ^{16}C , respectively. The enlarged part, which is able to discriminate the elastic and inelastic channels, is inserted in (b).

shown in Fig. 2(b). The red histogram in Fig. 2(b) represents the cut of ^{16}C (3σ) which was used to select elastic and inelastic scattering channels in this paper.

The energies of the recoil protons and deuterons, which were detected in coincidence with ^{16}C by the telescope T2, as a function of their angles in the laboratory frame are shown in Figs. 3(a) and 3(b), respectively. The red solid curves are the calculated kinematical ones for the elastic scattering channels. The dot-dashed lines correspond to the inelastic scattering to the 2_1^+ state at $E_x = 1.766$ MeV. It was found that most events are consistent with the kinematical curves, which indicates that these events are indeed from the elastic/inelastic scattering channels. However, a great deal of events with lower energies or at larger angles are lower than the solid curves because the energy losses in the thick target could not be ignored for the lower-energy protons and deuterons. In Fig. 3(a), it was found that although the statistics are limited, the 2_1^+ state is clearly separated from the ground state within this angular domain. As shown in the inserted picture in Fig. 3(b), the 2_1^+ state and the ground state are mixed at angles larger than 72° , which can be attributed to the larger energy dispersion in the thick $(\text{CD}_2)_n$ target, but the separation of these two states is realized at angles smaller than 72° .

For the $(\text{CD}_2)_n$ target, we found some proton events in the ΔE - E spectrum detected by the telescope T2. These events are in agreement with the kinematics of elastic scattering of $^{16}\text{C} + p$, which indicates that the $(\text{CD}_2)_n$ target was contaminated with hydrogen. In Fig. 3(b), the proton events were discarded using the ΔE - E spectrum in order to see the deuteron scattering events more clearly. The angular correlation spectra between forward-moving ^{16}C and all recoil light-charged particles from the $(\text{CH}_2)_n$ and $(\text{CD}_2)_n$ targets are shown in Figs. 4(a) and 4(b), respectively. In addition to the deuteron component, the hydrogen impurity was also clearly seen in Fig. 4(b). The ratio of proton and deuteron counts was determined to be $10.2 \pm 1.0(\text{stat}) \pm 1.2(\text{syst})\%$ using the method described in Ref. [37]. The statistic error 1.0% was

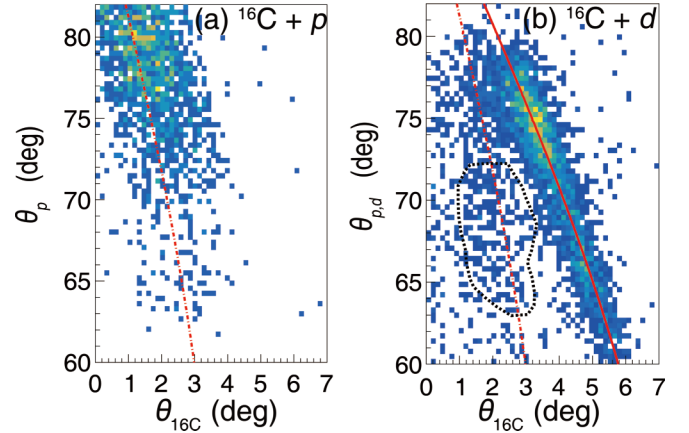


FIG. 4. Angular correlation spectra between ^{16}C and all the recoil light-charged particles from the $(\text{CH}_2)_n$ (a) and $(\text{CD}_2)_n$ (b) target. The red dot-dashed and solid lines are the calculated angular correlated curves of $^{16}\text{C} + p$ and $^{16}\text{C} + d$, respectively. The region marked by the black dotted curves in (b) represents the cut used to count the hydrogen numbers in the $(\text{CD}_2)_n$ target.

obtained from the numbers of counts for the scattered light particles and the incoming beam particles. The systematic error of 1.2% was determined from the different cuts using in Fig. 4(b) and the uncertainties in target thickness.

Figure 5 (Fig. 6) shows the Q -value spectrum deduced from the energies and angles of the recoil protons (deuterons) emitting to the angles of 63° - 74° (60° - 73°) in the laboratory frame. The protons and deuterons were chosen from the ΔE - E spectra measured by the DSSD and SSD [or SSD + CsI(Tl)] in the telescope T2. Obviously, the elastic scattering channel to $^{16}\text{C}_{\text{g.s.}}$ and inelastic scattering channel to the 2_1^+ state in ^{16}C can be discriminated from the Q -value spectra.

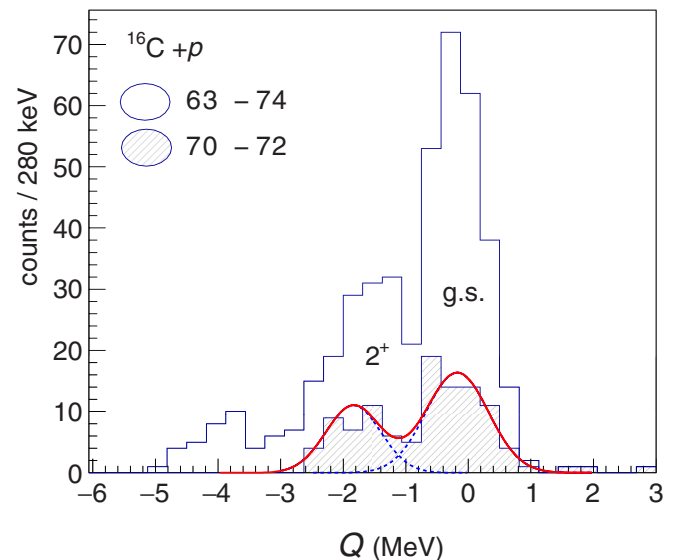


FIG. 5. Q -value spectrum obtained from the energies and angles of the recoil protons in coincidence with ^{16}C . The blue and green histograms represent the protons emitting to the angles of 63° - 74° and 70° - 72° , respectively.

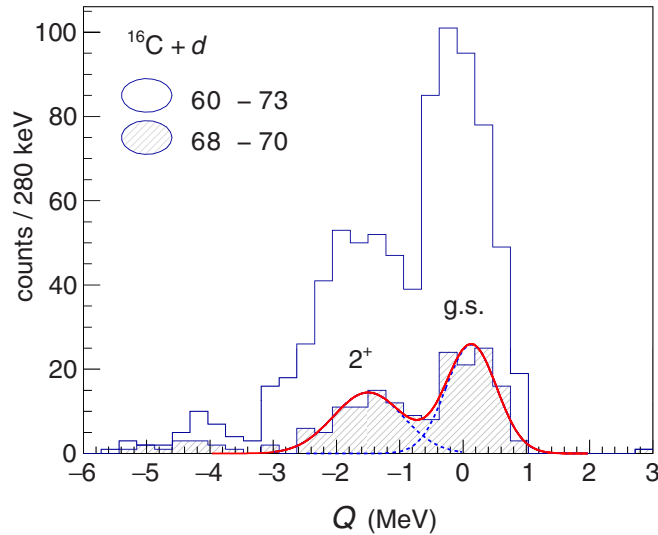


FIG. 6. Same as Fig. 5, but deduced from the recoil deuterons.

The full width at half-maximum (FWHM) of the Q value for the 2_1^+ state was 1.10 MeV for the proton target and 1.40 MeV for the deuteron target, which are in fair agreement with the simulation results using the GEANT4 package [41]. Six (three) Q -value spectra were constructed within an angular bin of 2° (2° – 4°) in the laboratory frame for the deuteron (proton) target. Different angular bins for the inelastic scattering of $^{16}\text{C}+p$ were chosen after the consideration of both the angular resolution of detectors and the statistical error of proton yield. The counts of the elastically or inelastically scattered protons (or deuterons) were determined by fitting each Q -value spectrum with two Gaussian functions. The typical ones are shown as green shadows in Figs. 5 and 6.

It is worth noting that the angular coverage of DCSs for the elastic and inelastic scattering channels are different due to the following reasons. According to the kinematics (see Fig. 3), the maximum emitting angle of the recoil protons (deuterons) from the inelastic scattering of ^{16}C is 74° (78°) in the laboratory frame. It means that the protons (deuterons) measured at angles larger than 74° (78°) completely come from the elastic scattering of ^{16}C . In order to identify deuterons from the ΔE - E spectrum, the lowest energy required for deuterons is 8.6 MeV. The deuteron with this energy just punch through the half-thickness of the target and the 300- μm DSSD, which is corresponding to 73° and 76° for the inelastic and elastic scattering of $^{16}\text{C}+d$, respectively. Thus, for angles larger than 73° in the laboratory frame, we only extracted the elastic scattering DCSs of $^{16}\text{C}+d$.

C. Elastic scattering

The elastic scattering DCSs, relative to the Rutherford DCSs, of ^{16}C from protons and deuterons are illustrated as solid circles in Figs. 7(a) and 7(b), respectively. Only the statistical errors are shown in Fig. 7, including the errors from the numbers of elastically scattered protons/deuterons and the incoming ^{16}C , as well as from the subtraction of the carbon background. The systematical errors were estimated to

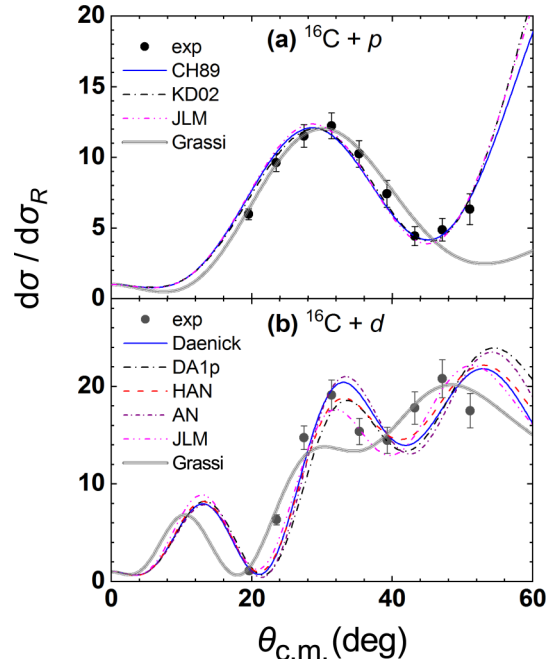


FIG. 7. Experimental and calculated elastic scattering DCSs, as a ratio to the Rutherford cross sections, for $^{16}\text{C}+p$ (a) and $^{16}\text{C}+d$ (b). The thin curves are from the coupled channel calculations using different global OPs with their corresponding normalization factors. The grey solid curves are the best-fit ones for the experimental angular distributions using larger diffuseness parameters in the Woods-Saxon potential. See text for more details.

be less than 10% for the $(\text{CH}_2)_n$ and $(\text{CD}_2)_n$ target, taking into account the uncertainties in geometrical efficiency determination (solid angles), the thickness of the target, the PID gate of ^{16}C as shown in Fig. 2(b), and the cuts applied on the Q -value spectra.

We applied the global optical potentials (OP) CH89 [42] and KD02 [43] to calculate the proton angular distributions, while the systematics obtained from Daehnick *et al.* [44], An *et al.* [45], Han *et al.* [46], and Zhang *et al.* (DA1p) [47] were applied to the deuteron DCSs. A single-folding model (SFM) with the Lane-consistent Bruy'eres Jeukenne-Lejeune-Mahaux (JLM) nucleon-nucleon interaction was also applied to describe these two sets of elastic scattering data. The energy-dependence parameters are obtained from Ref. [48]. The density distribution of ^{16}C calculated from the Hartree-Fock method using the SKX interaction [49] yields a matter radius of 2.68 fm, which is consistent with the values of 2.70 ± 0.03 fm and 2.64 ± 0.05 fm deduced from the interaction cross sections at incident energies of 960 MeV/nucleon [50] and 83 MeV/nucleon [51], respectively, and close to the value of 2.73 ± 0.03 fm given in Ref. [52]. In order to best fit the experimental data, the normalization factors, λ_R and λ_I , respectively, were applied to the well depths of real (V_V) and imaginary part ($W_V + W_S$) [36]. The searching process for the best λ_R and λ_I were performed with the code SFRESKO [53] using the χ^2 minimization method. All calculations using the normalized OPs show reasonable agreement with the corresponding experimental

DCSs. These normalized OPs were used as the starting points to search for another set of parameters in order to simultaneously reproduce the elastic and inelastic scattering channels with the coupled channel method.

For the imaginary part, two larger diffuseness parameters, 1.20 and 1.70 fm, were deduced from the elastic scattering of $^{16}\text{C}+p$ and $^{16}\text{C}+d$ at 50 MeV/nucleon by Grassi *et al.* [35]. Bonaccorso and Carstoiu suggested that these anomalously large diffuseness parameters were directly related to the anomalous structure of ^{16}C [35,54]. In order to check the necessity, we also applied a Woods-Saxon potential with six parameters V_V , a_R , r_R , W_V , a_I , and r_I to fit our experimental DCSs. The larger diffuseness parameters for the imaginary and real parts were, respectively, fixed to be $a_I = 1.20$ (1.70) fm and $a_R = 0.85$ (0.95) fm for the proton (deuteron) elastic scattering [35]. The standard radius parameters $r_R = r_I = 1.20$ fm were adopted. The well depths, V_V and W_V , were left as free parameters to fit the experimental data with the χ^2 minimization method. The optimal depths for the real and imaginary parts are $V_V = 25.33$ and $W_V = 8.03$ MeV for $^{16}\text{C}+p$, as well as $V_V = 68.82$ and $W_V = 14.29$ MeV for $^{16}\text{C}+d$. The optimal fit results are shown as grey solid lines in Fig. 7. For the angular distributions of $^{16}\text{C}+p$ [Fig. 7(a)], the grey solid line at larger angles is obviously different from these from the global potentials, and also remarkably deviates from the experimental points. For the DCSs of $^{16}\text{C}+d$ [Fig. 7(b)], the whole shape of grey solid line is clearly deviated from the experimental data, especially at the second maximum. The calculated TRCS for the system of $^{16}\text{C}+d$ ($^{16}\text{C}+p$) using larger diffuseness parameters is 1684 (730) mb. The value of 1684 mb is dramatically larger than those (≈ 900 mb) obtained from the global deuteron OPs, and also larger than the experimental value of 962 mb measured for $^{16}\text{O}+d$ at $E_{in} = 37.9$ MeV [55]. The TRCS of 730 mb is also larger than ≈ 550 mb measured for $^{16}\text{O}+p$ at $E_{in} = 24.6$ MeV [56]. Overall, the global OPs seem to provide a better reproduction of the elastic scattering data of $^{16}\text{C}+p$ and $^{16}\text{C}+d$ than the grey solid lines, demonstrating that the anomalously large diffuseness parameters are not necessary. The requirement of larger diffuseness parameters in Ref. [35] maybe due to inclusive measurements of the recoil protons and deuterons (without coincidence of ^{16}C), the lack of beam tracking information, and the unseparation of elastic and inelastic scattering channels.

D. Inelastic scattering

In Fig. 8(a) [Fig. 8(b)], we show the differential cross sections for the inelastic proton (deuteron) scattering to the 2_1^+ state. Only the statistical errors are shown in Fig. 8. The systematic errors were estimated to be about 12%, which is larger than the elastic scattering data due to a relatively larger influence of different fits to choose the 2_1^+ state. The carbon background and impurity proton in the $(\text{CD}_2)_n$ target have been subtracted after normalizing the number of incident ^{16}C and the target thickness.

Coupled channel calculations were performed using the code FRESKO [53] in the framework of rotational model to extract the deformation length from the inelastic scattering data,

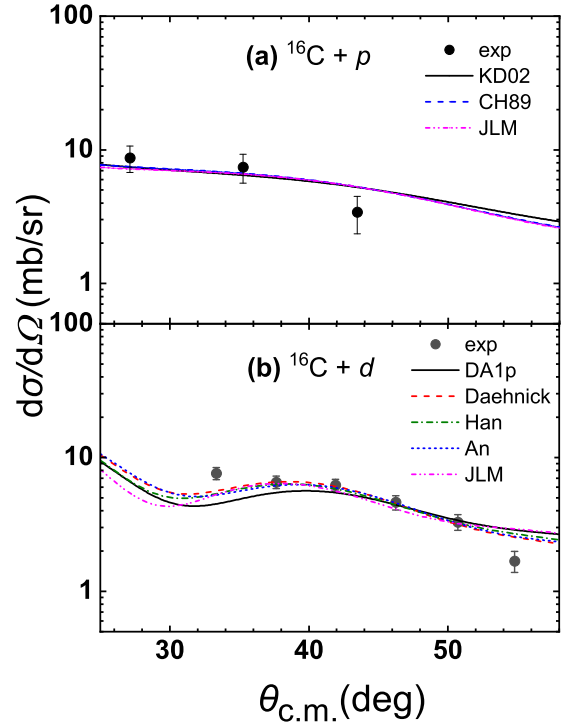


FIG. 8. The experimental angular distributions of inelastic proton (a) and deuteron (b) scattering of ^{16}C in comparison with the coupled channel calculations using different global OPs with their corresponding optimal normalization factors and deformation lengths. See text for more details.

similar to the method used for $^9\text{Li}+d$ [57] and $^{38}\text{S}+p$ [31]. Using $\delta = 1.0$ fm and the normalized OP parameters obtained from the elastic scattering data as the starting points, the normalization factors for the real and imaginary part (λ_R and λ_I), as well as the deformation length (δ) were left as free parameters, and were determined using the code SFRESKO [53] with the minimum χ^2 method. The searching process aims to simultaneously reproduce the elastic and inelastic scattering DCSs. The optimal results are given in Table II. Compared with the normalization factors obtained from elastic scattering DCSs, we found that the depth of the real part increases by about 2%, while that of the imaginary part decreases by about 10–15%. The average matter deformation lengths of $\delta_m^p = 1.22 \pm 0.25(\text{stat.}) \pm 0.07(\text{syst.})$ fm and $\delta_m^d = 1.18 \pm 0.15(\text{stat.}) \pm 0.06(\text{syst.})$ fm were deduced by normalizing the calculations to the experimental DCSs of proton and deuteron inelastic scattering to the 2_1^+ state in ^{16}C , respectively. The statistical errors were obtained from the experimental DCSs, while the systematic ones were deduced from the results with different OPs used in the calculations. The $\delta_m^p = 1.22 \pm 0.25 \pm 0.07$ fm determined from this experiment using the missing mass method with a thin 4.37 ± 0.05 mg/cm 2 $(\text{CH}_2)_n$ target is consistent with that of 1.44 ± 0.17 fm extracted from the inelastic proton scattering data using the γ -rays detection with a thick 225 ± 8 mg/cm 2 liquid hydrogen target [17].

Together with the elastic and inelastic scattering data (solid circles), the calculated results with the best normalized OPs and deformation lengths using the coupled channel method

TABLE II. Optimal normalization factors, deformation lengths, as well as the minimum χ^2 values from the coupled channel calculations using different OPs to simultaneously fit the elastic and inelastic scattering angular distributions. The upper (lower) part is for the systems of $^{16}\text{C} + p$ ($^{16}\text{C} + d$). The uncertainties of the normalization factors are shown in parentheses.

Global OPs	λ_R	λ_I	χ_{el}^2/n	χ_{inel}^2/n	δ (fm)
CH89 [42]	1.11(12)	0.83(9)	1.77	1.34	1.25(24)
KD02 [43]	1.14(12)	0.86(9)	1.17	1.38	1.15(23)
JLM [48]	1.11(12)	0.82(9)	2.15	1.45	1.26(25)
Average					$\delta_m^p=1.22(25)$
Dahenick [44]	0.93(10)	0.87(9)	7.96	2.85	1.18(15)
DA1p [47]	0.96(10)	0.84(9)	11.59	15.2	1.14(15)
Han [46]	1.14(12)	1.02(11)	8.42	3.76	1.20(16)
An [45]	0.91(10)	0.81(9)	12.0	3.38	1.15(15)
JLM [48]	1.01(11)	1.09(11)	6.17	6.84	1.24(16)
Average					$\delta_m^d=1.18(15)$

are shown as curves in Figs. 7 and 8, respectively. All calculations using different global OPs with the corresponding optimal λ_R , λ_I , and δ give satisfactory reproductions of the elastic and inelastic scattering angular distributions at the same time.

As shown in Eq. (3), for the 2_1^+ state, the ratio of the neutron and proton transition matrix element M_n/M_p can be deduced from the matter deformation length obtained with different reactions [25]. For the inelastic proton (neutron) scattering at incident energies between 10 and 50 MeV, the interaction strength is $b_n^p/b_p^p = 3$ ($b_n^n/b_p^n = 1/3$) [25]. For other probes, b_n^F and b_p^F depend on the ratios of N^F/A^F and Z^F/A^F , and the interaction strengths between neutrons and protons, referred to as b_n^n , b_n^p , b_p^n , and b_p^p [20],

$$b_n^F = \frac{N^F}{A^F} b_n^n + \frac{Z^F}{A^F} b_n^p, \quad (4)$$

$$b_p^F = \frac{N^F}{A^F} b_p^n + \frac{Z^F}{A^F} b_p^p. \quad (5)$$

For the inelastic deuteron scattering, $b_n^d/b_p^d = 1$ [29]. Therefore, for ^{16}C , we have

$$\frac{\delta_m^p}{\delta_p} = \frac{1 + 3M_n^p/M_p^p}{6}, \quad (6)$$

$$\frac{\delta_m^d}{\delta_p} = \frac{1 + M_n^d/M_p^d}{2.667}, \quad (7)$$

$$\frac{\delta_m^p}{\delta_m^d} = 0.44 \frac{1 + 3M_n^{pd}/M_p^{pd}}{1 + M_n^{pd}/M_p^{pd}}. \quad (8)$$

First, we extracted M_n/M_p with δ_p taken from other measurements. Together with $\delta_p = 0.98 \pm 0.20$ fm, the mean value obtained from the $B(E2)$ values of the latest three measurements [18,19,21], $M_n^p/M_p^p = 2.16 \pm 0.60$ ($M_n^d/M_p^d = 2.21 \pm 0.53$) was extracted from the deformation length of $\delta_m^p = 1.22 \pm 0.25$ fm ($\delta_m^d = 1.18 \pm 0.15$ fm) using Eq. (6) [Eq. (7)]. Then, $M_n^{pd}/M_p^{pd} = 1.95 \pm 0.47$ was deduced from

the present inelastic proton and deuteron scattering data using Eq. (8). This result is independent of other experimental data, and is consistent with M_n^p/M_p^p and M_n^d/M_p^d within error bars. M_n^{pd}/M_p^{pd} also reasonably agrees with these obtained from the probes of “ $B(E2) +$ previous proton inelastic scattering” and with inelastic scattering data from “proton + Pb”, see Table I. This implies that the combination of proton and neutron inelastic scattering is a useful method to extract M_n/M_p of even-even nuclei without help of other experimental results. These consistent values of $M_n/M_p \approx 1.20N/Z$ are larger than N/Z expected in a homogenous quantum liquid-drop model, indicating that the neutron contribution is larger than the proton contribution to the quadrupole collective excitation. Such larger contributions of neutrons have also been observed in the neighboring even-even semimagic nuclei $^{18,20}\text{O}$ [26,27].

Using $M_n/M_p = N\delta_n/(Z\delta_p)$, the equations of $\delta_m^p = (6\delta_p + 30\delta_n)/36$ and $\delta_m^d = (6\delta_p + 10\delta_n)/16$ were deduced from Eqs. (6) and (7), respectively. These two equations were utilized to determine δ_p and δ_n for the probe of “proton + deuteron”. Using Eq. (2) and the deduced proton deformation length of $\delta_p = 1.07 \pm 0.26$ fm, the $B(E2;2_1^+ \rightarrow 0_{g.s.})$ value is determined to be $4.34_{-1.85}^{+2.27} e^2 \text{fm}^4$, which agrees well with these from the latest three lifetime measurements [18,19,21]. The neutron deformation length $\delta_n = 1.25 \pm 0.30$ fm is consistent with that of $\delta_n = 1.37 \pm 0.12$ fm obtained from the probe of “proton + Pb” [20].

E. Theoretical calculations

Shell model calculations were performed for ^{16}C using MK [58], WBT [59], WBT* [59,60], and YSOX [61] interactions in p - sd model space [61,62]. Together with the experimental results, the calculated ratio of proton and neutron matrix elements M_n/M_p and $B(E2;2_1^+ \rightarrow 0_{g.s.})$ are listed in Table III. The results from a simple shell model calculation performed by Fortune [63] are also listed in Table III. Most of the calculated M_n/M_p values are below or close to the 1σ upper limit of $M_n/M_p = 1.95 \pm 0.47$ obtained from the present experiment.

TABLE III. The M_n/M_p and $B(E2;2_1^+ \rightarrow 0_{g.s.})$ values calculated from the shell model with different interactions, the *ab initio* IM-SRG, and the *ab initio* shell model.

Interaction	M_n/M_p	$B(E2;2_1^+ \rightarrow 0_{g.s.})$ ($e^2 \text{fm}^4$)
MK [62]	2.11	5.49
WBT[62]	2.47	4.18
WBT* [62]	2.53	3.90
YSOX [61]	2.48	3.02
H.T.Fortune [63]	3.0	4.05
<i>Ab initio</i> IM-SRG	2.54	2.58
<i>Ab initio</i> shell model [68]		2.4 ± 0.9
present	1.95 ± 0.47	$4.34_{-1.85}^{+2.27}$
		$4.21_{-0.26}^{+0.34}(\text{stat})$ [21]
		4.15 ± 0.73 [19]
		$2.6 \pm 0.2 \pm 0.7$ [18]

The *ab initio* IM-SRG [64–66] calculations were performed for ^{16}C using the optimized nucleon-nucleon interaction from chiral effective field theory at next-to-next-to-leading order [67]. A basis of 13 major shells with $\hbar\omega = 28$ MeV was applied. The single shell valence space interaction and operator with respect to ensemble states above ^{10}He were constructed and used in this calculation. The calculated excitation energy of the 2_1^+ state in ^{16}C is $E_x = 1.89$ MeV, which is close to the experimental value. The calculated $M_n/M_p = 2.54$ is also close to the value extracted from the present experiment.

III. SUMMARY

In summary, a new experiment of the proton/deuteron elastic and inelastic scattering has been performed in inverse kinematics with a 24 MeV/nucleon radioactive ^{16}C beam in order to study the quadrupole transition of $0_{\text{g.s.}}^+ \rightarrow 2_1^+$. The normalization factors for the depths of real and imaginary parts are adopted to better reproduce the elastic scattering DCSS of $^{16}\text{C}+p$ and $^{16}\text{C}+d$. The neutron and proton deformation lengths of $\delta_n = 1.25 \pm 0.30$ fm and $\delta_p = 1.07 \pm 0.26$ fm determined from this experiment, are in fair agreement with the former results. The ratio of neutron and proton transition matrix element $M_n/M_p = 1.95 \pm 0.47$ obtained from the

present elastic and inelastic scattering data using the probe of “proton + deuteron”, is consistent with the previous measurements. Most of the theoretical predictions by the shell model using different interactions in *p-sd* model space and the *ab initio* IM-SRG calculations are close to these experimental results. It is worth noting that these results are obtained from a new experiment using two different targets, proton and deuteron. This demonstrates that inelastic scattering data from this combined probe is a useful method to extract M_n/M_p for the even-even nuclei. In the future, this method will be used to study the collective excitation mode for more neutron- or proton-rich nuclei, such as $^{10,18,20}\text{C}$.

ACKNOWLEDGMENTS

We gratefully thank the IMP accelerator group for providing the ^{18}O primary beam and the RIBLL collaboration for supplying a lot of electronics. We also thank Prof. H. T. Fortune for calculating M_n/M_p in a simple shell model. This work was supported by the National Key R&D Program of China (Grant No. 2018YFA0404403), and the National Natural Science Foundation of China (Contracts No. 11775004, No. U1867214, No. 11775013, No. 11775316, No. 11535004, No. 11875074, and No. 11875073), and Hirose International Scholarship Foundation.

-
- [1] I. Tanihata, H. Savajols, and R. Kanungo, *Prog. Part. Nucl. Phys.* **68**, 215 (2013).
- [2] T. Nakamura, H. Sakurai, and H. Watanabe, *Prog. Part. Nucl. Phys.* **97**, 53 (2017).
- [3] D. T. Tran, H. J. Ong, G. Hagen, T. D. Morris, N. Aoi, T. Suzuki, Y. Kanada-En’yo, L. S. Geng, S. Terashima *et al.*, *Nat. Commun.* **9**, 1594 (2018).
- [4] T. Furuno, T. Kawabata, S. Adachi, Y. Ayyad, Y. Kanada-En’yo, Y. Fujikawa, K. Inaba, M. Murata, H. J. Ong, M. Sferrazza, Y. Takahashi, T. Takeda, I. Tanihata, D. T. Tran, and M. Tsumura, *Phys. Rev. C* **100**, 054322 (2019).
- [5] D. Dell’Aquila, I. Lombardo, L. Acosta, R. Andolina, L. Audatore, G. Cardella, M. B. Chatterjee, E. De Filippo, L. Francalanza *et al.*, *Phys. Rev. C* **93**, 024611 (2016).
- [6] N. Soić, M. Freer, L. Donadille, N. M. Clarke, P. J. Leask, W. N. Catford, K. L. Jones, D. Mahboub, B. R. Fulton, B. J. Greenhalgh, D. L. Watson, and D. C. Weisser, *Phys. Rev. C* **68**, 014321 (2003).
- [7] Z. Y. Tian, Y. L. Ye, Z. H. Li, C. J. Lin, Q. T. Li, Y. C. Ge, J. L. Lou, W. Jiang, J. Li *et al.*, *Chin. Phys. C* **40**, 1674 (2016).
- [8] J. Li, Y. L. Ye, Z. H. Li, C. J. Lin, Q. T. Li, Y. C. Ge, J. L. Lou, Z. Y. Tian, W. Jiang *et al.*, *Phys. Rev. C* **95**, 021303(R) (2017).
- [9] Hong-Liang Zang, Yan-Lin Ye, Zhi-Huan Li, Jian-Song Wang, Jian-Ling Lou, Qi-Te Li, Yu-Cheng Ge, Xiao-Fei Yang, Jing Li *et al.*, *Chin. Phys. C* **42**, 074003 (2018).
- [10] Jun Feng, YanLin Ye, Biao Yang, ChengJian Lin, HuiMin Jia, DanYang Pang, ZhiHuan Li, JianLing Lou, QiTe Li *et al.*, *Sci. China Phys. Mech. Astron.* **62**, 012011 (2019).
- [11] N. Furutachi and M. Kimura, *Phys. Rev. C* **83**, 021303(R) (2011).
- [12] X. X. Sun, J. Zhao, and S. G. Zhou, *Phys. Lett. B* **785**, 530 (2018).
- [13] M. Rashdan, *Phys. Rev. C* **86**, 044610 (2012).
- [14] Y. Kanada-En’yo, *Phys. Rev. C* **71**, 014310 (2005).
- [15] N. Imai, H. J. Ong, N. Aoi, H. Sakurai, K. Demichi, H. Kawasaki, H. Baba, Zs. Dombrádi, Z. Elekes, N. Fukuda, Z. Fulop, A. Gelberg, T. Gomi, H. Hasegawa, K. Ishikawa, H. Iwasaki, E. Kaneko, S. Kanno, T. Kishida, Y. Kondo, T. Kubo, K. Kurita, S. Michimasa, T. Minemura, M. Miura, T. Motobayashi, T. Nakamura, M. Notani, T. K. Onishi, A. Saito, S. Shimoura, T. Sugimoto, M. K. Suzuki, E. Takeshita, S. Takeuchi, M. Tamaki, K. Yamada, K. Yoneda, H. Watanabe, and M. Ishihara, *Phys. Rev. Lett.* **92**, 062501 (2004).
- [16] Z. Elekes, Z. Dombrádi, A. Krasznahorkay, H. Baba, M. Csatlós, L. Csige, N. Fukuda, Zs. Fülöp, Z. Gácsi *et al.*, *Phys. Lett. B* **586**, 34 (2004).
- [17] H. J. Ong, N. Imai, N. Aoi, H. Sakurai, Zs. Dombrádi, A. Saito, Z. Elekes, H. Baba, K. Demichi, Z. S. Fulop, J. Gibelin, T. Gomi, H. Hasegawa, M. Ishihara, H. Iwasaki, S. Kanno, S. Kawai, T. Kubo, K. Kurita, Y. U. Matsuyama, S. Michimasa, T. Minemura, T. Motobayashi, M. Notani, S. Ota, H. K. Sakai, S. Shimoura, E. Takeshita, S. Takeuchi, M. Tamaki, Y. Togano, K. Yamada, Y. Yanagisawa, and K. Yoneda, *Phys. Rev. C* **73**, 024610 (2006).
- [18] H. J. Ong, N. Imai, D. Suzuki, H. Iwasaki, H. Sakurai, T. K. Onishi, M. K. Suzuki, S. Ota, S. Takeuchi *et al.*, *Phys. Rev. C* **78**, 014308 (2008).
- [19] M. Wiedeking, P. Fallon, A. O. Macchiavelli, J. Gibelin, M. S. Basunia, R. M. Clark, M. Cromaz, M.-A. Deleplanque, S. Gros *et al.*, *Phys. Rev. Lett.* **100**, 152501 (2008).

- [20] Z. Elekes, N. Aoi, Zs. Dombrádi, Zs. Fülöp, T. Motobayashi, and H. Sakurai, *Phys. Rev. C* **78**, 027301 (2008).
- [21] M. Petri, S. Paschalis, R. M. Clark, P. Fallon, A. O. Macchiavelli, K. Starosta, T. Baugher, D. Bazin, L. Cartegni *et al.*, *Phys. Rev. C* **86**, 044329(R) (2012).
- [22] P. Voss, T. Baugher, D. Bazin, R. M. Clark, H. L. Crawford, A. Dewald, P. Fallon, A. Gade, G. F. Grinyer *et al.*, *Phys. Rev. C* **86**, 011303(R) (2012).
- [23] Z. Elekes, Zs. Dombrádi, T. Aiba, N. Aoi, H. Baba, D. Bemmerer, B. A. Brown, T. Furumoto, Zs. Fülöp, N. Iwasa, A. Kiss, T. Kobayashi, Y. Kondo, T. Motobayashi, T. Nakabayashi, T. Nannichi, Y. Sakuragi, H. Sakurai, D. Sohler, M. Takashina, S. Takeuchi, K. Tanaka, Y. Togano, K. Yamada, M. Yamaguchi, and K. Yoneda, *Phys. Rev. C* **79**, 011302(R) (2009).
- [24] M. Petri, P. Fallon, A. O. Macchiavelli, S. Paschalis, K. Starosta, T. Baugher, D. Bazin, L. Cartegni, R. M. Clark *et al.*, *Phys. Rev. Lett.* **107**, 102501 (2011).
- [25] A. M. Bernstein, V. A. Madsen, and V. R. Brown, *Comments Nucl. Part. Phys.* **11**, 203 (1983).
- [26] J. K. Jewell, L. A. Riley, P. D. Cottle, K. W. Kemper, T. Glasmacher, R. W. Ibbotson, H. Scheit, M. Chromik, Y. Blumenfeld *et al.*, *Phys. Lett. B* **454**, 181 (1999).
- [27] E. Khan, Y. Blumenfeld, Nguyen Van Giai, T. Suomijärvi, N. Alamanos, F. Auger, G. Colò, N. Frascaria, A. Gillibert *et al.*, *Phys. Lett. B* **490**, 45 (2000).
- [28] J. S. Randhawa, R. Kanungo, M. Holl, J. D. Holt, P. Navrátil, S. R. Stroberg, G. Hagen, G. R. Jansen, M. Alcorta, C. Andreoiu, C. Barnes, C. Burbadge, D. Burke, A.A. Chen, A. Chester, G. Christian, S. Cruz, B. Davids, J. Even, G. Hackman, J. Henderson, S. Ishimoto, P. Jassal, S. Kaur, M. Keefe, D. Kisliuk, R. Krucken, J. Liang, J. Lighthall, E. McGee, J. Measures, M. Moukaddam, E. Padilla-Rodal, A. Shotton, I.J. Thompson, J. Turko, M. Williams, and O. Workman, *Phys. Rev. C* **99**, 021301(R) (2019).
- [29] N. Iwasa, T. Motobayashi, S. Bishop, Z. Elekes, J. Gibelin, M. Hosoi, K. Ieki, K. Ishikawa, H. Iwasaki *et al.*, *Phys. Rev. C* **78**, 024306 (2008).
- [30] S. Takeuchi, N. Aoi, T. Motobayashi, S. Ota, E. Takeshita, H. Suzuki, H. Baba, T. Fukui, Y. Hashimoto *et al.*, *Phys. Rev. C* **79**, 054319 (2009).
- [31] J. H. Kelley, T. Suomijärvi, S. E. Hirzebruch, A. Azhari, D. Bazin, Y. Blumenfeld, J. A. Brown, P. D. Cottle, S. Danczyk *et al.*, *Phys. Rev. C* **56**, R1206 (1997).
- [32] T. Marchi, G. de Angelis, J. J. Valiente-Dobón, V. M. Bader, T. Baugher, D. Bazin, J. Berryman, A. Bonaccorso, R. Clark, A. Bonaccorso, R. Clark, L. Coraggio, H. L. Crawford, M. Doncel, E. Farnea, A. Gade, A. Gadea, A. Gargano, T. Glasmacher, A. Gottardo, F. Gramegna, N. Itaco, P. R. John, R. Kumar, S. M. Lenzi, S. Lunardi, S. McDaniel, C. Michelagnoli, D. Mengoni, V. Modamio, D. R. Napoli, B. Quintana, A. Ratkiewicz, F. Recchia, E. Sahin, R. Stroberg, D. Weisshaar, K. Wimmer, and R. Winkler, *Phys. Rev. Lett.* **113**, 182501 (2014).
- [33] S. Raman, C. W. Nestor, and P. Tikkanen, *At. Data Nucl. Data Tables* **78**, 1 (2001).
- [34] M. Takashina, Y. Kanada-En'yo, and Y. Sakuragi, *Phys. Rev. C* **71**, 054602 (2005).
- [35] L. Grasi, C. Agodi, F. Amorini, A. Anzalone, L. Audatore, G. Cardella, M. B. Chatterjee, E. DeFilippo, E. Geraci *et al.*, *J. Phys.: Conf. Ser.* **381**, 012088 (2012).
- [36] J. Chen, J. L. Lou, Y. L. Ye, Z. H. Li, Y. C. Ge, Q. T. Li, J. Li, W. Jiang, Y. L. Sun *et al.*, *Phys. Rev. C* **93**, 034623 (2016).
- [37] J. Chen, J. L. Lou, Y. L. Ye, J. Rangel, A. M. Moro, D. Y. Pang, Z. H. Li, Y. C. Ge, Q. T. Li *et al.*, *Phys. Rev. C* **94**, 064620 (2016).
- [38] J. Chen, J. L. Lou, Y. L. Ye, Z. H. Li, D. Y. Pang, C. X. Yuan, Y. C. Ge, Q. T. Li, H. Hua *et al.*, *Phys. Lett. B* **781**, 412 (2018).
- [39] J. Chen, J. L. Lou, Y. L. Ye, Z. H. Li, D. Y. Pang, C. X. Yuan, Y. C. Ge, Q. T. Li, H. Hua *et al.*, *Phys. Rev. C* **98**, 014616 (2018).
- [40] S. Carboni, S. Barlini, L. Bardelli *et al.*, *Nucl. Instrum. Methods Phys. Res. A* **664**, 251 (2012).
- [41] S. Agostinelli, J. Allison, and K. Amako, *Nucl. Instrum. Methods Phys. Res. A* **506**, 250 (2003).
- [42] R. L. Varner, *Phys. Rep.* **201**, 57 (1991).
- [43] A. J. Koning and J. P. Delaroche, *Nucl. Phys. A* **713**, 231 (2003).
- [44] W. W. Daehnick, J. D. Childs, and Z. Vrcelj, *Phys. Rev. C* **21**, 2253 (1980).
- [45] H. X. An and C. H. Cai, *Phys. Rev. C* **73**, 054605 (2006).
- [46] Y. L. Han, Y. Y. Shi, and Q. B. Shen, *Phys. Rev. C* **74**, 044615 (2006).
- [47] Y. Zhang, D. Y. Pang, and J. L. Lou, *Phys. Rev. C* **94**, 014619 (2016).
- [48] D. Y. Pang, Y. L. Ye, and F. R. Xu, *Phys. Rev. C* **83**, 064619 (2011).
- [49] B. A. Brown, *Phys. Rev. C* **58**, 220 (1998).
- [50] A. Ozawa, O. Bochkarev, L. Chulkov, D. Cortina, H. Geissel, M. Hellström, M. Ivanov, R. Janik, K. Kimurae *et al.*, *Nucl. Phys. A* **691**, 599 (2001).
- [51] T. Zheng, T. Yamaguchi, A. Ozawa, M. Chiba, R. Kanungo, T. Kato, K. Katori, K. Morimoto, T. Ohnishi *et al.*, *Nucl. Phys. A* **709**, 103 (2002).
- [52] R. Kanungo, W. Horiuchi, G. Hagen, G. R. Jansen, P. Navrátil, F. Ameil, J. Atkinson, Y. Ayyad, D. Cortina-Gil *et al.*, *Phys. Rev. Lett.* **117**, 102501 (2016).
- [53] I. J. Thompson, *Comput. Phys. Rep.* **7**, 167 (1988).
- [54] A. Bonaccorso and F. Carstoiu, *Nucl. Phys. A* **706**, 322 (2002).
- [55] A. Auce, R. F. Carlson, A. J. Cox, A. Ingemarsson, R. Johansson, P. U. Renberg, O. Sundberg, and G. Tibell, *Phys. Rev. C* **53**, 2919 (1996).
- [56] I. Slaus, D. J. Margaziotis, R. F. Carlson, W. T. H. van Oers, and J. Reginald Richardson, *Phys. Rev. C* **12**, 1093 (1975).
- [57] H. Al Falou, R. Kanungo, C. Andreoiu, D. S. Cross, B. Davids, M. Djongolov, A. T. Gallant, N. Galinski, D. Howell *et al.*, *Phys. Lett. B* **721**, 224 (2013).
- [58] D. J. Millener and D. Kurath, *Nucl. Phys. A* **255**, 315 (1975).
- [59] E. K. Warburton and B. A. Brown, *Phys. Rev. C* **46**, 923 (1992).
- [60] D. Sohler, M. Stanoiu, Zs. Dombrádi, F. Azaiez, B. A. Brown, M. G. Saint-Laurent, O. Sorlin, Yu.-E. Penionzhkevich, N. L. Achouri, J. C. Angélique, M. Bellegruic, C. Borcea, C. Bourgeois, J. M. Daugas, F. DeOliveira-Santos, Z. Dlouhy, C. Donzaud, J. Duprat, Z. Elekes, S. Grevy, D. Guillemaud-Mueller, F. Ibrahim, S. Leenhardt, M. Lewitowicz, M. J. Lopez-Jimenez, S. M. Lukyanov, W. Mittig, J. Mrazek, F. Negoita, Z. Podolyak, M. G. Porquet, F. Pougheon, P. Roussel-Chomaz, H. Savajols, G. Sletten, Y. Sobolev, C. Stodel, and J. Timar, *Phys. Rev. C* **77**, 044303 (2008).
- [61] C. Yuan, T. Suzuki, T. Otsuka, F. Xu, and N. Tsunoda, *Phys. Rev. C* **85**, 064324 (2012).

- [62] C. X. Yuan, C. Qi, and F. R. Xu, *Nucl. Phys. A* **883**, 25 (2012).
- [63] H. T. Fortune, *Phys. Rev. C* **93**, 044322 (2016).
- [64] S. K. Bogner, H. Hergert, J. D. Holt, A. Schwenk, S. Binder, A. Calci, J. Langhammer, and R. Roth, *Phys. Rev. Lett.* **113**, 142501 (2014).
- [65] S. R. Stroberg, A. Calci, H. Hergert, J. D. Holt, S. K. Bogner, R. Roth, and A. Schwenk, *Phys. Rev. Lett.* **118**, 032502 (2017).
- [66] B. S. Hu, Q. Wu, Z. H. Sun, and F. R. Xu, *Phys. Rev. C* **99**, 061302(R) (2019).
- [67] A. Ekström, G. Baardsen, C. Forssén, G. Hagen, M. Hjorth-Jensen, G. R. Jansen, R. Machleidt, W. Nazarewicz, T. Papenbrock, J. Sarich, and S. M. Wild, *Phys. Rev. Lett.* **110**, 192502 (2013).
- [68] C. Forssén, R. Roth, and P. Navrátil, *J. Phys. G: Nucl. Part. Phys* **40**, 055105 (2013).